

**¹⁰Be**原子核微观团簇结构研究

曹颖逾 陶德晔 周波

Microscopic Cluster Study of the ¹⁰Be Nucleus

CAO Yingyu, TAO Deye, ZHOU Bo

在线阅读 View online: <https://doi.org/10.11804/NuclPhysRev.41.2023CNPC87>

引用格式:

曹颖逾, 陶德晔, 周波. ¹⁰Be原子核微观团簇结构研究[J]. 原子核物理评论, 2024, 41(1):148–155. doi: 10.11804/NuclPhysRev.41.2023CNPC87CAO Yingyu, TAO Deye, ZHOU Bo. Microscopic Cluster Study of the ¹⁰Be Nucleus[J]. Nuclear Physics Review, 2024, 41(1):148–155. doi: 10.11804/NuclPhysRev.41.2023CNPC87

您可能感兴趣的其他文章

Articles you may be interested in[通过费米能区重离子碰撞产额分布来研究¹⁶O原子核的团簇结构](#)Probing Clustering Configurations of ¹⁶O by the Yield Distribution in Heavy Ion Collisions at Fermi Energy
原子核物理评论. 2021, 38(1): 8–16 <https://doi.org/10.11804/NuclPhysRev.38.2020057>[氦团簇及氦间隙原子在钨中的稳定性研究](#)Study on the Stability of Helium Clusters and Interstitials of Helium in Tungsten
原子核物理评论. 2019, 36(2): 256–260 <https://doi.org/10.11804/NuclPhysRev.36.02.256>[低能Cu₁₃团簇沉积薄膜的分子动力学模拟研究](#)Molecular Dynamics Simulation Study on the Film Formation by Low Energy Cu₁₃ Clusters Deposition
原子核物理评论. 2019, 36(2): 235–241 <https://doi.org/10.11804/NuclPhysRev.36.02.235>[基于统一方法描述原子核的alpha衰变、结团放射性和冷裂变](#)Unified Description of the Competition Between α Decay, Cluster Radioactivity and Cold Fission
原子核物理评论. 2023, 40(3): 348–355 <https://doi.org/10.11804/NuclPhysRev.40.2022004>[低温高密核物质测量谱仪时间投影室的集团重建](#)Cluster Reconstruction for the CSR External-target Experiment (CEE) Time Projection Chamber
原子核物理评论. 2021, 38(4): 416–422 <https://doi.org/10.11804/NuclPhysRev.38.2021021>[宇宙核素¹⁰Be、⁷Be、²²Na大气示踪概述](#)Overview of Atmospheric Tracing by Using Cosmogenic Nuclides of ¹⁰Be, ⁷Be, ²²Na
原子核物理评论. 2021, 38(3): 277–282 <https://doi.org/10.11804/NuclPhysRev.38.2020073>

Microscopic Cluster Study of the ^{10}Be Nucleus

CAO Yingyu¹, TAO Deye¹, ZHOU Bo^{1,2,†}

(*1. Institute of Modern Physics, Fudan University, Shanghai 200433, China;*

2. Shanghai Research Center for Theoretical Nuclear Physics, NSFC and Fudan University, Shanghai 200438, China)

Abstract: Using a microscopic four-body cluster model, we investigate the spectral properties and structural configurations of the ^{10}Be nucleus. We calculate physical quantities such as the root-mean-squared (r.m.s.) radii and electromagnetic transition strengths. The theoretical results for the energies and certain electromagnetic transition strengths of the low-lying states show good agreement with experimental data. In particular, the enhancement of the r.m.s. radius and isoscalar monopole transition strength of the 0_3^+ state indicates a well-developed cluster structure. We obtained three 1^- states in $E_x < 15$ MeV that show remarkable dipole transition strengths, suggesting that the 1^- states may have cluster structure. Using the obtained wave functions, we calculate the reduced-width amplitudes (RWAs) to investigate the $^6\text{He} + \alpha$ and $^9\text{Be} + n$ two-body cluster structures in ^{10}Be . The results suggest that the low-lying states show the two-body $^6\text{He} + \alpha$ and $^9\text{Be} + n$ configuration, with the $^6\text{He} + \alpha$ components of the two-body structure diminishing as the energy increases, which due to the breakup of ^6He and ^9Be at higher excitation energies. Moreover, a few states above the $\alpha + \alpha + n + n$ threshold still exhibit significant $^9\text{Be} + n$ components.

Key words: cluster model; cluster structure; electromagnetic transition strengths

CLC number: O571.6

Document code: A

DOI: [10.11804/NuclPhysRev.41.2023CNPC87](https://doi.org/10.11804/NuclPhysRev.41.2023CNPC87)

0 Introduction

Nuclear clustering is a universal phenomenon in light nuclei^[1–3]. The α cluster can be considered one of the most stable subunits in light nuclei^[4]. More than half a century ago, Ikeda and Horiuchi proposed that α -clustering structures can occur near the α threshold of $A = 4N$ nuclei^[5]. For example, the ground state of ^8Be exhibits a structure of two α clusters, while the well-known Hoyle state (0_2^+) of ^{12}C consists of three α clusters^[6–8]. Currently, the search for Hoyle-analog states, such as 4α and 5α , has garnered significant attention^[9–12].

More and more research show that there are also rich cluster structures^[13–14] in non-conjugate atomic nuclei. The ^{10}Be nucleus can be considered as one typical case with the $2\alpha + 2n$ clustering structure. Many experiments take much efforts to investigate the clustering structure of ^{10}Be . In Ref. [15], the characteristics of high-lying excited states of ^{10}Be up to 18.80 MeV were explored via the $^9\text{Be}(^9\text{Be}, ^{10}\text{Be})^8\text{Be}$ reaction, and new resonance states at 15.6 MeV and 18.8 MeV were found from the $\alpha + ^6\text{He}$ and $t + ^7\text{Li}$ decay channels. Moreover, two-proton pick-up reactions^[16–17] $^{12}\text{C}(^6\text{He}, ^8\text{Be})^{10}\text{Be}$ and $^{12}\text{C}(^{12}\text{C}, ^{14}\text{O})^{10}\text{Be}$ dis-

cussed the structure of the rotational bands. Recent experimental studies^[14] show even the ground state of ^{10}Be can be described by a dumbbell-shaped 2α core (with moderate extension) surrounded by the two valence neutrons occupying the π orbit.

On the other hand, various theoretical models have been used to study the structure of ^{10}Be , including shell models^[18–21], nuclear cluster models^[22–26] and some *ab initio* methods^[27–29]. In Ref. [30], the shell model calculations with $4\hbar\omega$ model space with a microscopic effective nucleon-nucleon interactions, and it did not well reproduce the energy levels of ^{10}Be . Moreover, the 0_2^+ state, considered an intruder state, cannot be described by simple shell model methods.

Within microscopic cluster models, the studies indicated that many states of Be isotopes have 2α clustering structure. In Refs. [31–34], it was found that the developed 2α clustering structure in the ground state of ^8Be weakens in ^{10}Be due to the valence neutrons. The antisymmetrized molecular dynamics (AMD) discussed the band structure as $K^\pi = 0_1^+, 0_2^+, 1^-,$ and 2^+ . It is found that the molecular-like states with the developed 2α structure construct the rotational bands $K^\pi = 0_2^+$ and 1^- with small level spacing,

Received date: 12 Jan. 2024; **Revised date:** 12 Feb. 2024

Foundation item: National Key R&D Program of China (2022YFA1602402); Shanghai "Science and Technology Innovation Action Plan" Natural Science Foundation Project (21ZR1409500)

Biography: CAO Yingyu(1995–), male, Shanghai, Graduate student, Working on nuclear cluster physics

† Corresponding author: ZHOU Bo, Email: zhou_bo@fudan.edu.cn

which is supported by the experimental energy level. Recently, the AMD under a constrain on the deformation parameter^[35] analyzed the single particle orbits of the valence neutrons. It was found that the main component of the valence neutrons which are around two α clusters seems to be the σ orbit for the negative parity of ^{10}Be . The resonating group method (RGM) described the $\alpha + \alpha + n + n$ four-body wave function of ^{10}Be ^[36], and the calculation indicated that the 2^- state has a polarized ^9Be core, influenced by molecular-like configurations, but well decouple from the s -wave valence neutron, making it a clear candidate for an excited state neutron halo. Furthermore, in Ref. [37], the wave function of ^{10}Be is a superposition of various spatial configurations and deformations, including clustering of $^5\text{He} + ^5\text{He}$, $^6\text{He} + \alpha$, $^7\text{Li} + ^3\text{H}$, $^8\text{Be} + 2n$, and $^9\text{Be} + n$. More recently, The Tohsaki-Horiuchi-Schuck-Röpke (THSR) wave function^[38–39] was extended to describe ^{10}Be ^[40] within a new nonlocalized picture. It is found that the 0_1^+ and 0_2^+ states calculated by a single THSR wave function are consistent with other models as well as with experimental results.

In the present work, we aim to conduct studies on the clustering structure of the ground and excited states of ^{10}Be . The $\alpha + \alpha + n + n$ configuration is included within generator coordinate method (GCM) framework.

The paper is organized as follows: in Sec. I, we explain the framework of the GCM and the computational details. In Sec. II, we present and discuss the results for the ground and excited states of ^{10}Be . The key conclusions of this study are summarized in Sec. III.

1 Theoretical framework

The ^{10}Be is described by four-body cluster model, involving two α particles and two valence neutrons. The $\alpha + \alpha + n + n$ configuration is illustrated in Fig. 1.

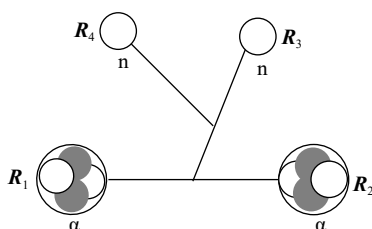


Fig. 1 Schematic diagram of $\alpha + \alpha + n + n$ clustering configuration of ^{10}Be .

The Brink wave function^[41] is used as the basis wave function for $\alpha + \alpha + n + n$ configuration as follows,

$$\begin{aligned}\Phi(\mathbf{R}_1, \mathbf{R}_2, \mathbf{R}_3, \mathbf{R}_4) &= \mathcal{A}(\Phi_a(\mathbf{R}_1)\Phi_a(\mathbf{R}_2)\Phi_n(\mathbf{R}_3)\Phi_n(\mathbf{R}_4)), \\ \Phi_a(\mathbf{R}) &= \mathcal{A} \left\{ \prod_{i=1}^4 \phi(\mathbf{R}, \mathbf{r}_i) \chi_i \tau_i \right\}, \\ \Phi_n(\mathbf{R}) &= \phi(\mathbf{R}, \mathbf{r}) \chi_i \tau_i \\ \phi(\mathbf{R}, \mathbf{r}_i) &= \left(\frac{1}{\pi b^2} \right)^{3/4} e^{-\frac{(\mathbf{r}_i - \mathbf{R})^2}{2b^2}},\end{aligned}\quad (1)$$

where Φ_a and Φ_n are the wave functions of the α particle and valence neutron, respectively. \mathbf{R}_1 , \mathbf{R}_2 , \mathbf{R}_3 and \mathbf{R}_4 are the generator coordinates of two α and two valence neutrons, abbreviated as $\{\mathbf{R}\} = \{\mathbf{R}_1, \mathbf{R}_2, \mathbf{R}_3, \mathbf{R}_4\}$. The condition $(4\mathbf{R}_1 + 4\mathbf{R}_2 + \mathbf{R}_3 + \mathbf{R}_4)/10 = 0$ is applied. $\phi(\mathbf{R}, \mathbf{r}_i) \chi_i \tau_i$ represents the i -th single-particle wave function, where $\phi(\mathbf{R}, \mathbf{r}_i)$ is the spatial wave function. χ_i and τ_i denote the spin of two valence neutrons is set to up and down, respectively. The oscillator width $b = 1.46$ fm is chosen for all clusters to avoid the spurious center-of-mass problem in this work. Assuming that the two valence neutrons are placed in the same position ($\mathbf{R}_3 = \mathbf{R}_4$), Eq. (1) simplifies to the tri-cluster wave function of $\alpha + \alpha + 2n$. Similarly, $\alpha + ^6\text{He}$ configuration can be constructed by positioning one α closer to the two valence neutrons.

The GCM wave functions of ^{10}Be are obtained by superposing over various $\alpha + \alpha + n + n$ configuration, which can be written as

$$Y_M^{J\pi} = \sum_{\{\mathbf{R}\}K} f_{\{\mathbf{R}\}K} \Phi_{MK}^{J\pi}(\{\mathbf{R}\}), \quad (2)$$

where $\Phi_{MK}^{J\pi}(\{\mathbf{R}\})$ is the projected wave functions,

$$\Phi_{MK}^{J\pi}(\{\mathbf{R}\}) = P_{MK}^J P^\pi \Phi(\{\mathbf{R}\}). \quad (3)$$

P_{MK}^J and P^π denote the parity and angular momentum projector, respectively. The coefficients $f_{\{\mathbf{R}\}K}$ are determined by solving the Hill-Wheeler equation^[42], which is given by

$$\sum_{\{\mathbf{R}'\}K'} f_{\{\mathbf{R}\}K} \left[\langle \Phi_{MK}^{J\pi}(\{\mathbf{R}\}) | \hat{H} | \Phi_{MK'}^{J\pi}(\{\mathbf{R}'\}) \rangle - E \langle \Phi_{MK}^{J\pi}(\{\mathbf{R}\}) | \Phi_{MK'}^{J\pi}(\{\mathbf{R}'\}) \rangle \right] = 0. \quad (4)$$

The Hamiltonian employed in this study is as follows,

$$\hat{H} = \sum_{i=1}^{10} t_i - t_{\text{c.m.}} + \sum_{i < j}^{10} V_{ij}^{NN} + \sum_{i < j}^{10} V_{ij}^C, \quad (5)$$

where t_i denotes the kinetic energy operator for the i -th nucleon, while $t_{\text{c.m.}}$ corresponds to the kinetic energy operator for the center-of-mass. We adopted the Volkov No.2 interaction^[43] combined with the G3RS potential^[44–45] as the nucleon-nucleon interaction, which is given as

$$V_{ij}^{NN} = \sum_{n=1}^2 V_n e^{-r_{ij}^2/a_n^2} (W + BP_\sigma - HP_\tau - MP_\sigma P_\tau) + \sum_{n=1}^2 w_n e^{-b_n r_{ij}^2} P(^3O) \mathbf{L} \cdot \mathbf{S}, \quad (6)$$

where P_σ and P_τ stand for the spin and isospin exchange operators, respectively. $V_1 = -60.65$ MeV, $V_2 = 61.14$ MeV, $a_1 = 1.80$ fm, $a_2 = 1.01$ fm, $W = 1 - M$, $M = 0.60$, and $B = H = 0.125$. For the two-body spin-orbit force, $P(^3O)$ represents the projection operator to the triplet-odd states, $b_1 = 5.0$ fm $^{-2}$, $b_2 = 2.778$ fm $^{-2}$, and $w_1 = -w_2 = 2000$ MeV.

To study the two-body clustering structure in ^{10}Be , we calculate the reduced width amplitudes (RWAs) in the $\alpha + ^6\text{He}$ and $^9\text{Be} + n$ channels. The RWAs in two-body channel is defined as

$$Y_{j_1\pi_1,j_2\pi_2,j_{12}}^{J\pi}(a) = \sqrt{\frac{A!}{(1 + \delta_{C_1C_2})C_1!C_2!}} \times \left\langle \frac{\delta(r-a)}{r^2} \left[Y_l(\hat{r}) \left[\Phi_{C_1}^{j_1\pi_1} \Phi_{C_2}^{j_2\pi_2} \right]_{j_{12}} \right]_{JM} \right| \Psi_M^{J\pi} \rangle, \quad (7)$$

where $\Phi_{C_1}^{j_1\pi_1}$ and $\Phi_{C_2}^{j_2\pi_2}$ are the wave functions of cluster C_1 and C_2 . The spins j_1 of cluster C_1 and j_2 of cluster C_2 are coupled to j_{12} , then the j_{12} is coupled to the orbital angular momentum l of the relative-motion function to yield the total spin-parity J^π . The parity π_1 , π_2 and the orbital angular momentum l satisfy the relation $\pi = \pi_1\pi_2(-)^l$. More details can be found in Refs. [46–48].

The ISM transition has been regarded as a powerful probe to identify the developed cluster states [49–52] and is defined by

$$\mathcal{M}^{\text{ISM}} = \sum_{i=1}^{10} (\mathbf{r}_i - \mathbf{r}_{\text{c.m.}})^2. \quad (8)$$

The isoscalar dipole (ISD) transitions as another probe for studying asymmetric cluster structures [53–55]. The operator and transition strength are defined as follows,

$$\mathcal{M}^{\text{ISD}} = \sum_{i=1}^{10} (\mathbf{r}_i - \mathbf{r}_{\text{c.m.}})^3 Y_{1\mu}(\mathbf{r}_i - \widehat{\mathbf{r}}_{\text{c.m.}}), \quad (9)$$

$$B(\text{ISD}; J_i \rightarrow J_f) = \sum_{M_f, \mu} |\langle J_f M_f | \mathcal{M}_\mu^{\text{ISD}} | J_i M_i \rangle|^2, \quad (10)$$

where J_i and J_f are the angular momentums of the initial state $|J_i M_i\rangle$ and final state $|J_f M_f\rangle$, respectively. \mathbf{r}_i and $\mathbf{r}_{\text{c.m.}}$ denote the coordinate of the i -th nucleon and the center of mass of the system, respectively. The $Y_{1\mu}$ represents the solid spherical harmonics of degree 1 and order μ .

The electric dipole and quadrupole transition strengths $B(E1)$ and $B(E2)$ are important observational quantities, which can be represented as follows,

$$\mathcal{M}_\mu^{E\lambda} = e^2 \sum_{i=1}^{10} \frac{1 - \tau_{iz}}{2} (\mathbf{r}_i - \mathbf{r}_{\text{c.m.}})^i Y_{\lambda\mu}(\mathbf{r}_i - \widehat{\mathbf{r}}_{\text{c.m.}}), \quad (11)$$

$$B(E\lambda; J_i \rightarrow J_f) = \sum_{M_f, \mu} |\langle J_f M_f | \mathcal{M}_\mu^{E\lambda} | J_i M_i \rangle|^2, \quad (12)$$

where τ_{iz} is the isospin projection of the i -th nucleon.

2 Results and discussion

We performed GCM calculations by superposing 1 200 basis wave functions. The calculated energy spectrum is compared with experimental data and real-time evolution method (REM) results from Ref. [56], as shown in Fig. 2.

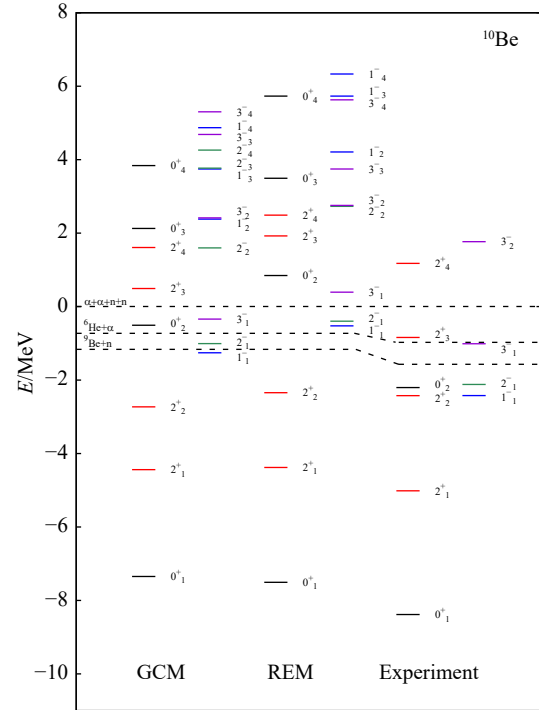


Fig. 2 The calculated and experimental energy spectra of ^{10}Be . (color online)

For the low-lying states, the calculated ground state energy is slightly higher than that from REM calculations. However, for the bound 2_1^+ and 2_2^+ states, the calculated energies are lower than those of REM. The calculated energies of the 1_1^- , 2_2^- and 3_1^- states are below the $\alpha + \alpha + n + n$ threshold and basically consistent with the experimental data, whereas the 3_1^- state energy is slightly higher the threshold for the REM calculation. Notably, both our calculations and REM fail to describe the experimental 2_3^+ state. For the high-lying states, the calculated energies of 2_4^+ and 3_2^- states agree with experimental results. On the whole, our results basically reproduce the current experimental energy spectrum for both positive and negative parity states and is consistent with the REM calculations.

The isoscalar monopole transition is a measure of probing cluster structures. As discussed in the Refs.

[51–52], the enhancement of monopole transitions strength reflect the degree of radial excitation from the excited cluster state to the ground state. In Table 1, we list the radii and ISM transition strengths based on present GCM calculations and AMD results. The ground state radius obtained from GCM calculation is 2.5 fm, which is consistent with the radius calculated by AMD. However, the radii of excited states of 0_2^+ and 0_3^+ calculated by AMD are larger than those of GCM. It is noted that both GCM and AMD calculations show enhancement in the monopole transition from the 0_3^+ state to the ground state. This enhancement indicated that the 0_3^+ state could be the well-developed cluster structure. Actually, in Ref. [57], they consider the 0_3^+ state would have a gaslike expanded dineutron nature.

Table 1 The radii (units: fm) of the ground (0_1^+) and excited states (0_2^+ and 0_3^+) and monopole transition strength (units: fm^4) from the excited states to the ground state. The AMD calculations are quoted from Ref. [33].

| Radius and transition | Present GCM | AMD |
|--|-------------|-----|
| $r_{\text{rms}} (0_1^+)$ | 2.5 | 2.5 |
| $r_{\text{rms}} (0_2^+)$ | 3.1 | 3.4 |
| $r_{\text{rms}} (0_3^+)$ | 3.0 | 3.7 |
| $B(\text{ISM}, 0_2^+ \rightarrow 0_1^+)$ | 7.4 | 5.9 |
| $B(\text{ISM}, 0_3^+ \rightarrow 0_1^+)$ | 8.8 | 8.6 |
| $B(\text{ISM}, 0_3^+ \rightarrow 0_2^+)$ | 2.5 | |

The significant low-energy dipole (LED) strengths may suggest the emergence of new excitation modes, typically interpreted as collective oscillations of the entire system. In Ref. [58], three 1^- states in $E_x < 15$ MeV were calculated using AMD+GCM with $\alpha + {}^6\text{He}$ and $\alpha + \alpha + 2n$ cluster model. They found the 1_1^- state is dominated by the $\alpha + {}^6\text{He}$ configuration, whereas the 1_2^- and 1_3^- states can be explained by three-body excitations of the $\alpha + \alpha + 2n$ clustering.

We calculated the isoscalar dipole transition strengths from the ground state to 1^- states using superposed $\alpha + \alpha + n + n$ wave function for comparison, and the results are listed in Table 2. We found that the 1_1^- , 1_2^- and 1_3^- states all exhibit strong ISD transition strengths. However, the 1_2^- state has a small ISD strength in Ref. [58]. This discrepancy may arise from different configurations, particularly, the present GCM calculation include $\alpha + \alpha + n + n$ configuration. In Ref. [58], only 198 $\alpha + {}^6\text{He}$ and $\alpha + \alpha + 2n$ basis functions were utilized, whereas we super-

Table 2 The isoscalar dipole transition strengths (units: fm^6) from ground state to the the excited states 1_1^- , 1_2^- and 1_3^- .

| Transition | Present GCM | Ref. [58] |
|--|-------------|-----------|
| $B(\text{ISD}, 0_1^+ \rightarrow 1_1^-)$ | 49.2 | 48.3 |
| $B(\text{ISD}, 0_1^+ \rightarrow 1_2^-)$ | 47.3 | 1.8 |
| $B(\text{ISD}, 0_1^+ \rightarrow 1_3^-)$ | 21.9 | 48.9 |

posed 1200 basis functions with $\alpha + \alpha + n + n$ configuration.

The $E1$ and $E2$ transition strengths can give the deformation to reflect the cluster structure of excited states. The results for GCM, AMD, shell model and experimental data of transition strengths $B(E1, 0_2^+ \rightarrow 1_1^-)$, $B(E2, 2_1^+ \rightarrow 0_1^+)$, and $B(E2, 0_2^+ \rightarrow 2_1^+)$ are presented in Table 3. The calculated $E1$ and $E2$ transition strengths agree well with the experimental data and close to the AMD calculation. For example, the experimental $B(E2)$ value is 10.5, while our calculated result is 11.72, and the AMD result is 11. In contrast, the shell model gives a significantly overestimated value of 16.26 [21].

Table 3 The $E1$ (units: efm^2) and $E2$ (units: $e^2\text{fm}^4$) transition strength $B(E1, 0_2^+ \rightarrow 1_1^-)$, $B(E2, 2_1^+ \rightarrow 0_1^+)$, and $B(E2, 0_2^+ \rightarrow 2_1^+)$ calculated by present GCM are compared with the experimental data, AMD calculations and shell model results. The shell model calculations are quoted from the work in Ref. [21].

| Transition | Expt. | Present GCM | AMD | Shell model |
|----------------------------------|------------------------------|----------------------|----------------------|-------------|
| $B(E2, 2_1^+ \rightarrow 0_1^+)$ | 10.5 ± 1.1 | 11.72 | 11 | 16.26 |
| $B(E2, 0_2^+ \rightarrow 2_1^+)$ | 3.3 ± 2.0 | 1.86 | 0.6 | 7.20 |
| $B(E1, 0_2^+ \rightarrow 1_1^-)$ | $1.3 \pm 0.6 \times 10^{-2}$ | 1.1×10^{-3} | 0.6×10^{-2} | |

2.1 Two-cluster configurations in ^{10}Be

The two-body structure of ${}^6\text{He} + \alpha$ and ${}^9\text{Be} + n$ configuration are important channels of ${}^{10}\text{Be}$ and have been studied in many works [36, 56–57]. By the use of Eq. (7), the RWAs of ${}^6\text{He}(0^+, 2^+) + \alpha$ and ${}^9\text{Be}(3/2^-, 1/2^+) + n$ configurations are calculated and the results are shown in Figs. 3~7. The RWAs measure the two-body clustering in the nuclei and can further serve as the input data to calculate the cross sections of reactions [59]. From the results we can see that, in the first two 0^+ states, the structure of ${}^6\text{He} + \alpha$ is well formed. The RWAs of the ground state is basically consistent with the REM result [56]. Notably, the ${}^6\text{He}(0^+) + \alpha$ curve, exhibiting two nodes in the ground state, is excited to three-node structure in the 0_2^+ state. The nodal excitation from the ground state to the 0_2^+ state has also been obtained by the calculation of Kobayashi *et al.* [57]. Analogically, the ${}^6\text{He}(2^+) + \alpha$ configuration present a one-node curve in the ground state, but two-node in the excited 0_2^+ state. In the ground state, the configurations of ${}^9\text{Be}(3/2^-) + n$ is comparable with ${}^6\text{He}(0^+) + \alpha$ and ${}^6\text{He}(2^+) + \alpha$, while the ${}^9\text{Be}(1/2^+) + n$ amplitude is negligible. In the higher 0^+ states, the amplitudes of ${}^9\text{Be} + n$ are further suppressed. Due to the complexity of angular-momentum coupling, more channels emerge in higher angular-momentum states of ${}^{10}\text{Be}$. Mainly three channels of ${}^6\text{He} + \alpha$ exist in the 2^+ states, namely $[{}^6\text{He}(0^+) + \alpha]_0 \otimes 2$, $[{}^6\text{He}(2^+) + \alpha]_2 \otimes 0$, and $[{}^6\text{He}(2^+) + \alpha]_2 \otimes 2$. The channels of $[{}^6\text{He}(0^+) + \alpha]_0 \otimes 2$ and $[{}^6\text{He}(2^+) + \alpha]_2 \otimes 2$ dominate in the

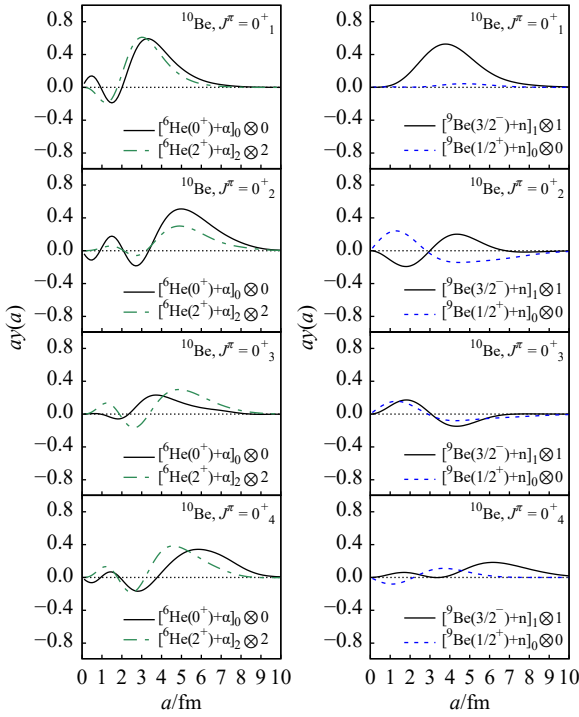


Fig. 3 The calculated RWAs of ^{10}Be for 0^+_1 , 0^+_2 , 0^+_3 , and 0^+_4 states. In the left panel are the RWAs of $[^6\text{He}(0^+)+\alpha]_0 \otimes 0$ and $[^6\text{He}(2^+)+\alpha]_2 \otimes 2$ channels. In the right panel are the RWAs of $[^9\text{Be}(3/2^-)+n]_1 \otimes 1$ and $[^9\text{Be}(1/2^+)+n]_0 \otimes 0$ channels. (color online)

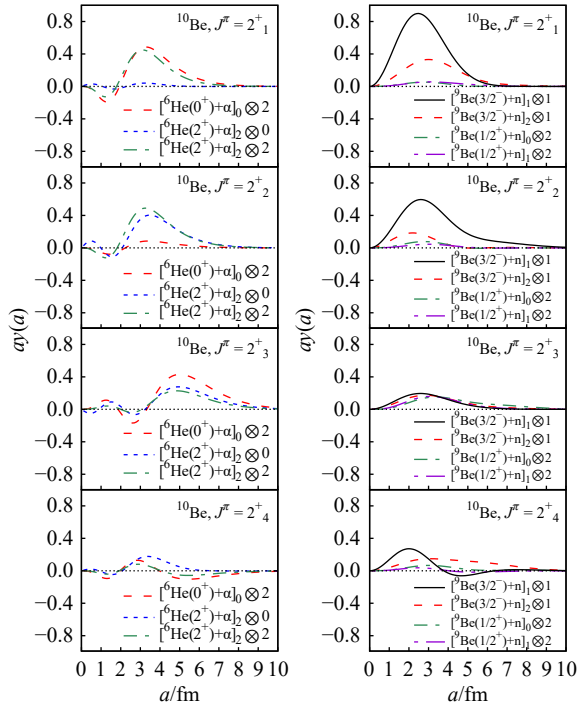


Fig. 4 The calculated RWAs of ^{10}Be for 2^+_1 , 2^+_2 , 2^+_3 , and 2^+_4 states. In the left panel are the RWAs of $[^6\text{He}(0^+)+\alpha]_0 \otimes 2$, $[^6\text{He}(2^+)+\alpha]_2 \otimes 0$, and $[^6\text{He}(2^+)+\alpha]_2 \otimes 2$ channels. In the right panel are the RWAs of $[^9\text{Be}(3/2^-)+n]_1 \otimes 1$, $[^9\text{Be}(3/2^-)+n]_2 \otimes 1$, $[^9\text{Be}(1/2^+)+n]_0 \otimes 2$, and $[^9\text{Be}(1/2^+)+n]_1 \otimes 2$ channels. (color online)

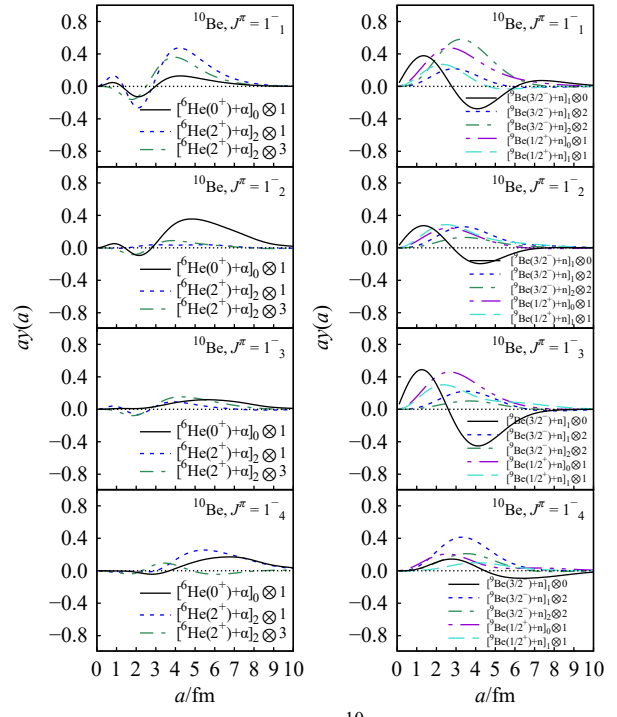


Fig. 5 The calculated RWAs of ^{10}Be for 1^-_1 , 1^-_2 , 1^-_3 , and 1^-_4 states. In the left panel are the RWAs of $[^6\text{He}(0^+)+\alpha]_0 \otimes 1$, $[^6\text{He}(2^+)+\alpha]_2 \otimes 1$, and $[^6\text{He}(2^+)+\alpha]_2 \otimes 3$ channels. In the right panel are the RWAs of $[^9\text{Be}(3/2^-)+n]_1 \otimes 0$, $[^9\text{Be}(3/2^-)+n]_1 \otimes 2$, $[^9\text{Be}(3/2^-)+n]_2 \otimes 2$, $[^9\text{Be}(1/2^+)+n]_0 \otimes 1$, and $[^9\text{Be}(1/2^+)+n]_1 \otimes 1$ channels. (color online)

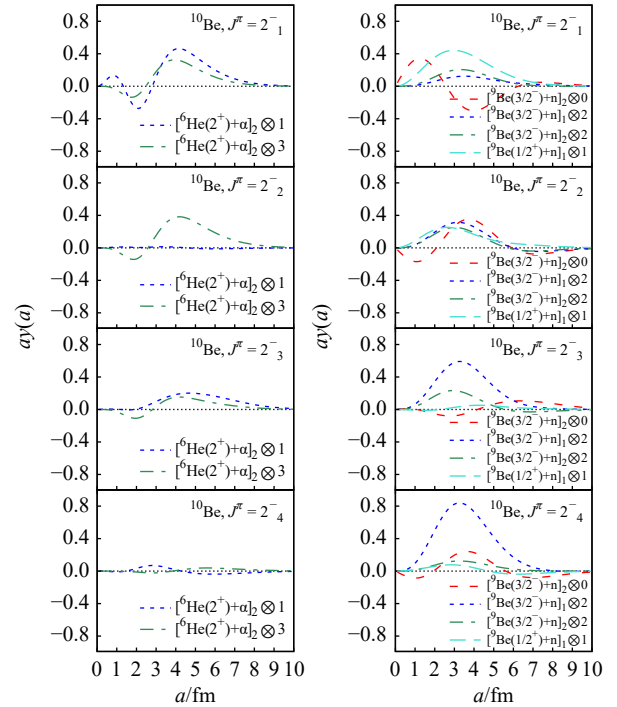


Fig. 6 The calculated RWAs of ^{10}Be for 2^-_1 , 2^-_2 , 2^-_3 , and 2^-_4 states. In the left panel are the RWAs of $[^6\text{He}(2^+)+\alpha]_2 \otimes 1$, and $[^6\text{He}(2^+)+\alpha]_2 \otimes 3$ channels. In the right panel are the RWAs of $[^9\text{Be}(3/2^-)+n]_2 \otimes 0$, $[^9\text{Be}(3/2^-)+n]_1 \otimes 2$, $[^9\text{Be}(3/2^-)+n]_2 \otimes 2$, and $[^9\text{Be}(1/2^+)+n]_1 \otimes 1$ channels. (color online)

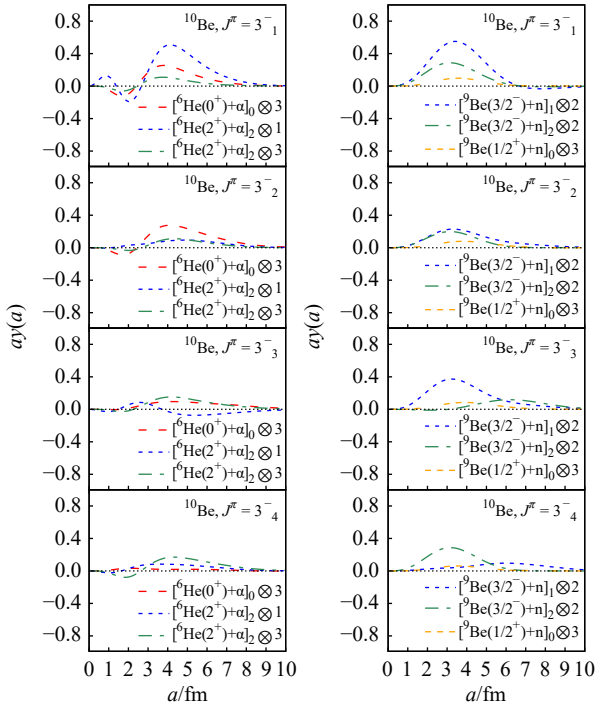


Fig. 7 The calculated RWAs of ^{10}Be for 3^-_1 , 3^-_2 , 3^-_3 , and 3^-_4 states. In the left panel are the RWAs of $[^6\text{He}(0^+)+\alpha]_0 \otimes 3$, $[^6\text{He}(2^+)+\alpha]_2 \otimes 1$, and $[^6\text{He}(2^+)+\alpha]_2 \otimes 3$ channels. In the right panel are the RWAs of $[^9\text{Be}(3/2^-)+n]_1 \otimes 2$, $[^9\text{Be}(3/2^-)+n]_2 \otimes 2$, and $[^9\text{Be}(1/2^+)+n]_0 \otimes 3$ channels. (color online)

2^+_1 state, while in the 2^+_2 state, the $[^6\text{He}(2^+)+\alpha]_2 \otimes 0$ and $[^6\text{He}(2^+)+\alpha]_2 \otimes 2$ channels are more significant. In the higher 2^+_3 state, the node-excitation of the above three channels can be observed. For the 2^+_4 state, all the three channels are obviously suppressed, as the result of that the state is too high above the $^6\text{He} + \alpha$ threshold. Meanwhile, in terms of the $^9\text{Be} + n$ structure, only the $[^9\text{Be}(3/2^-)+n]_1 \otimes 1$ channel is prominent in the 2^+_1 and 2^+_2 states. For the 2^+_3 and 2^+_4 states, all $^9\text{Be} + n$ configurations are insignificant.

In the lowest three negative states near the $^6\text{He} + \alpha$ and $^9\text{Be} + n$ thresholds, namely 1^-_1 , 2^-_1 , and 3^-_1 , the RWAs curves exhibit multi-configuration features, as in the lowest positive states 0^+_1 , 2^+_1 , and 2^+_2 . Notably, the arrangements of $^6\text{He} + \alpha$ structure channels are quite similar in the 1^-_1 and 2^-_1 states, both containing significant $[^6\text{He}(2^+)+\alpha]_2 \otimes 1$ and $[^6\text{He}(2^+)+\alpha]_2 \otimes 3$ components, which is consistent with the results obtained by Arai^[36]. Additionally, the $[^6\text{He}(2^+)+\alpha]_2 \otimes 1$ channel in the 3^-_1 state also exhibit the alike curve as in 1^-_1 and 2^-_1 . However, although still exhibit the one-node feature, the $[^6\text{He}(2^+)+\alpha]_2 \otimes 3$ curve in 3^-_1 is obviously reduced, compared with that in the 1^-_1 and 2^-_1 states. The $^9\text{Be} + n$ channels also show some common features in the 1^-_1 and 2^-_1 states, but behave differently in 3^-_1 . The $[^9\text{Be}(3/2^-)+n]_1 \otimes 0$ in 1^-_1 and $[^9\text{Be}(3/2^-)+n]_2 \otimes 0$ in 2^-_1 , as well as the $[^9\text{Be}(1/2^+)+n]_0 \otimes 1$ in 1^-_1 and $[^9\text{Be}(1/2^+)+n]_1 \otimes 1$ in 2^-_1 , exhibit analogical amplitudes, while the pattern of 3^-_1

distinct from that of 1^-_1 and 2^-_1 . Such characteristics, along with the fact that the 1^-_1 and 2^-_1 states are very close in the spectra, suggest the similarity between these two states in structure. The other higher negative states do not show significant $^6\text{He} + \alpha$ component, since most of the maximum amplitudes are less than 0.4. In these states, due to the high excited energy, are more likely to be dominated by three-body or four-body configurations. However, regarding the $^9\text{Be} + n$ structure, some of the high negative states exhibit pronounced core + n configurations. In the state 1^-_3 , significant $[^9\text{Be}(3/2^-)+n]_1 \otimes 0$ and $[^9\text{Be}(1/2^+)+n]_0 \otimes 1$ channels exist, exhibiting one-node and zero-node curves, respectively. Besides, the $[^9\text{Be}(3/2^-)+n]_1 \otimes 2$ configuration is prominent in both the 2^-_3 and 3^-_3 states.

3 Summary

The spectra and electromagnetic transition strengths of ^{10}Be are analysed using the microscopic four-body cluster model, in which the structure of $\alpha + \alpha + n + n$ is employed and several correlations between the clusters are considered. For the low-lying states, the results of our GCM calculation are consistent with that of the REM and experiments. The monopole transition strength indicates the existence of well-developed cluster structures in the 0^+_3 state, and the $E1$ and $E2$ transition strengths are consistent with AMD calculations.

The RWAs results show that, in most of the states below or around the two-body thresholds, the structures of $^6\text{He} + \alpha$ and $^9\text{Be} + n$ are both significant. As the energy increasing, the components of two-body structures are suppressed, which may be due to the breakup of ^6He and ^9Be at higher excitation energies. However, in a few states high above the $\alpha + \alpha + n + n$ threshold, prominent $^9\text{Be} + n$ channels exist.

Acknowledgments The work was supported by China National Key R&D Program (2022YFA1602402) and Shanghai "Science and Technology Innovation Action Plan" Natural Science Foundation Project (21ZR1409500).

References:

- [1] WILDERMUTH K, TANG Y C. A Unified Theory of the Nucleus[M]. Wiesbaden: Vieweg+Teubner Verlag, 1977.
- [2] IKEDA K, HORIUCHI H, SAITO S. *Prog Theor Phys Suppl*, 1981, 68: 1.
- [3] FREER M, HORIUCHI H, KANADA-EN'YO Y, et al. *Rev Mod Phys*, 2018, 90: 035004.
- [4] VON OERTZEN W, FREER M, KANADA-EN'YO Y. *Phys Rep*, 2006, 432(2): 43.
- [5] IKEDA K, TAKIGAWA N, HORIUCHI H. *Prog Theor Phys Suppl*, 1968, E68: 464.
- [6] HOYLE F. *The Astrophysical Journal Supplement Series*, 1954, 1: 121.

- [7] HORIUCHI H. *Prog Theor Phys*, 1975, 53(2): 447.
- [8] CHERNYKH M, FELDMEIER H, NEFF T, et al. *Phys Rev Lett*, 2007, 98: 032501.
- [9] HORIUCHI H, IKEDA K. *Prog Theor Phys*, 1968, 40(2): 277.
- [10] FUNAKI Y, HORIUCHI H, TOHSAKI A, et al. *Prog Theor Phys*, 2002, 108(2): 297.
- [11] FUNAKI Y, YAMADA T, HORIUCHI H, et al. *Phys Rev Lett*, 2008, 101: 082502.
- [12] ZHOU B, FUNAKI Y, HORIUCHI H, et al. *Nat Commun*, 2023, 14(1): 8206.
- [13] ZHUKOV M, DANILIN B, FEDOROV D, et al. *Phys Rep*, 1993, 231(4): 151.
- [14] LI P J, BEAUMEL D, LEE J, et al. *Phys Rev Lett*, 2023, 131: 212501.
- [15] WEI JIANG E A. *Sci Sin-Phys Mech Astron*, 2017, 60(6): 062011.
- [16] MILIN M, MILJANIĆ D, ALIOTTA M, et al. *Phys Rev C*, 2004, 70: 044603.
- [17] BOHLEN H G, DORSCH T, KOKALOVA T, et al. *Phys Rev C*, 2007, 75: 054604.
- [18] WOLTERS A A, VAN HEES A G M, GLAUDEMANS P W M. *Phys Rev C*, 1990, 42: 2062.
- [19] LIU L, OTSUKA T, SHIMIZU N, et al. *Phys Rev C*, 2012, 86: 014302.
- [20] MYO T, UMEYA A, TOKI H, et al. *Prog Theor Exp Phys*, 2015, 2015(6): 063D.
- [21] NAKADA H, OTSUKA T. *Phys Rev C*, 1994, 49: 886.
- [22] DESCOUNVEMONT P, ITAGAKI N. *Prog Theor Exp Phys*, 2020, 2020(2): 023D.
- [23] NISHIOKA H. *Journal of Physics G: Nuclear Physics*, 1984, 10(12): 1713.
- [24] ITAGAKI N, AOYAMA S, OKABE S, et al. *Phys Rev C*, 2004, 70: 054307.
- [25] ITAGAKI N, ITO M, MILIN M, et al. *Phys Rev C*, 2008, 77: 067301.
- [26] ITO M, KATO K, IKEDA K. *Phys Lett B*, 2004, 588(1): 43.
- [27] QUAGLIONI S, NAVRÁTIL P. *Phys Rev Lett*, 2008, 101: 092501.
- [28] CAPRIO M, MARIS P, VARY J. *Phys Lett B*, 2013, 719(1): 179.
- [29] MARIS P. *J Phys Conf Ser*, 2013, 445: 012035.
- [30] NAVRÁTIL P, BARRETT B R. *Phys Rev C*, 1998, 57: 3119.
- [31] ITO M. *AIP Conf Proc*, 2006, 853(1): 396.
- [32] FURUMOTO T, SUHARA T, ITAGAKI N. *Prog Theor Exp Phys*, 2023, 2023(6): 063D.
- [33] KANADA-EN'YO Y, HORIUCHI H, DOTÉ A. *Phys Rev C*, 1999, 60: 064304.
- [34] KANADA-EN'YO Y. *Phys Rev C*, 2016, 94: 024326.
- [35] DOTÉ A, HORIUCHI H, KANADA-EN'YO Y. *Phys Rev C*, 1997, 56: 1844.
- [36] ARAI K. *Phys Rev C*, 2004, 69: 014309.
- [37] MYO T, LYU M, ZHAO Q, et al. *Phys Rev C*, 2023, 108: 064314.
- [38] TOHSAKI A, HORIUCHI H, SCHUCK P, et al. *Phys Rev Lett*, 2001, 87: 192501.
- [39] ZHOU B, FUNAKI Y, HORIUCHI H, et al. *Phys Rev Lett*, 2013, 110: 262501.
- [40] LYU M, REN Z, ZHOU B, et al. *Phys Rev C*, 2016, 93: 054308.
- [41] BRINK D. The Alpha-Particle Model of Light Nuclei[C]//BLOCH C ed. Proceedings of the International School of Physics “Enrico Fermi” Course 36, Varenna, 1965. London: Academic Press, 1966: 247.
- [42] RING P, SCHUCK P. The Nuclear Many-body Problem[M]. Berlin: Springer Science & Business Media, 2004.
- [43] VOLKOV A. *Nucl Phys*, 1965, 74(1): 33.
- [44] YAMAGUCHI N, KASAHIRO T, NAGATA S, et al. *Prog Theor Phys*, 1979, 62(4): 1018.
- [45] OKABE S, ABE Y. *Prog Theor Phys*, 1979, 61(4): 1049.
- [46] LYU M, YOSHIDA K, KANADA-EN'YO Y, et al. *Phys Rev C*, 2018, 97: 044612.
- [47] LYU M, YOSHIDA K, KANADA-EN'YO Y, et al. *Phys Rev C*, 2019, 99: 064610.
- [48] CHIBA Y, KIMURA M. *Prog Theor Exp Phys*, 2017, 2017(5): 053D01.
- [49] YANG Z H, YE Y L, ZHOU B, et al. *Phys Rev Lett*, 2023, 131: 242501.
- [50] KAWABATA T, AKIMUNE H, FUJITA H, et al. *Phys Lett B*, 2007, 646(1): 6.
- [51] YAMADA T, FUNAKI Y, HORIUCHI H, et al. *Prog Theor Phys*, 2008, 120(6): 1139.
- [52] YAMADA T, FUNAKI Y, MYO T, et al. *Phys Rev C*, 2012, 85(3): 034315.
- [53] CHIBA Y, KIMURA M, TANIGUCHI Y. *Phys Rev C*, 2016, 93(3): 034319.
- [54] KANADA-EN'YO Y. *Phys Rev C*, 2016, 93(2): 024322.
- [55] CHIBA Y, TANIGUCHI Y, KIMURA M. *Phys Rev C*, 2017, 95(4): 044328.
- [56] ZHAO Q, KIMURA M, ZHOU B, et al. *Phys Rev C*, 2022, 106: 054313.
- [57] KOBAYASHI F, KANADA-EN'YO Y. *Phys Rev C*, 2012, 86: 064303.
- [58] SHIKATA Y, KANADA-EN'YO Y, MORITA H. *Prog Theor Exp Phys*, 2019, 2019(6): 063D.
- [59] BRIDA I, PIEPER S C, WIRINGA R B. *Phys Rev C*, 2011, 84: 024319.

^{10}Be 原子核微观团簇结构研究

曹颖逾¹, 陶德晔¹, 周波^{1,2,†}

(1. 复旦大学现代物理研究所, 上海 200433;
2. 国家自然科学基金理论物理专款-复旦大学上海核物理理论研究中心, 上海 200438)

摘要: 使用微观四体簇模型, 研究了 ^{10}Be 原子核的能谱和团簇结构。计算了物理量, 如均方根(r.m.s.)半径和电磁跃迁强度。低能态的能量和某些电磁跃迁强度的理论结果与实验数据吻合良好。我们的计算显示 0_3^+ 有显著的半径和标量单极子跃迁强度, 这些性质表明 0_3^+ 态有明显的团簇结构。在激发能 $E_x < 15 \text{ MeV}$ 范围内得到三个 1^- 态, 这些态表现出显著的偶极子跃迁强度, 暗示了 1^- 态可能存在团簇结构。利用获得的波函数, 计算了约化宽度振幅(RWAs)以研究 $^6\text{He} + \alpha$ 和 $^9\text{Be} + n$ 在 ^{10}Be 的两体团簇结构。RWAs的结果表明, 在 ^{10}Be 低能态中存在 $^6\text{He} + \alpha$ 和 $^9\text{Be} + n$ 的两体结构, 但随着能量升高, $^6\text{He} + \alpha$ 的成分会减小, 这可能是由于 ^6He 和 ^9Be 在较高激发能量下会破裂。此外, 有少量高于 $\alpha + \alpha + n + n$ 阈值的态依然存在显著 $^9\text{Be} + n$ 组分。

关键词: 团簇模型; 团簇结构; 电磁跃迁强度

收稿日期: 2024-01-12; 修改日期: 2024-02-12

基金项目: 国家重点研发计划项目(2022YFA1602402); 上海市“科技创新行动计划”自然科学基金项目(21ZR1409500)

†通信作者: 周波, E-mail: zhou_bo@fudan.edu.cn